Simulated Performance of Antenna Position Estimation through Sub-Sampled Exponential Analysis

Rina-Mari Weideman
Dept of Electrical & Electronic Engineering
Stellenbosch University
Stellenbosch, South Africa
18954626@sun.ac.za

Ridalise Louw
Dept of Electrical & Electronic Engineering
Stellenbosch University
Stellenbosch, South Africa
17002567@sun.ac.za

Ferre Knaepkens
Dept of Computer Science
University of Antwerp
Antwerp, Belgium
ferre.knaepkens@uantwerpen.be

Dirk de Villiers
Dept of Electrical & Electronic Engineering
Stellenbosch University
Stellenbosch, South Africa
ddv@sun.ac.za

Annie Cuyt
Dept of Computer Science
University of Antwerp
Antwerp, Belgium
annie.cuyt@uantwerpen.be

Wen-Shin Lee
Division of Computing Science and Mathematics
University of Stirling
Stirling, Scotland
wen-shin.lee@stir.ac.uk

Stefan J. Wijnholds
Dept of Research & Development
Netherlands Institute for Radio Astronomy (ASTRON)
Dept of Electrical & Electronic Engineering
Stellenbosch University
Dwingeloo, The Netherlands
wijnholds@astron.nl

***Abstract*—Antenna position estimation is an important problem in large irregular arrays where the positions might not be known very accurately from the start. In a previous paper we presented a method using harmonically related signals transmitted from an Unmanned Aerial Vehicle (UAV), with the added advantage that the UAV can be in the near-field of the receiving antenna array. It was shown that the method delivers excellent results using ideal synthetic data with added noise. In this paper we continue the work by simulating the problem in a full-wave solver. Although the results are less accurate than when synthetic data are used, due to the effects of mutual coupling, the method still performs satisfactorily, with errors smaller than 4% of the smallest transmitted wavelength.**

***Index Terms*—Antenna Arrays, Antenna Measurements, Mutual Coupling, Unmanned Aerial Vehicles**

I. Introduction

Large irregular antenna arrays such as the Low Frequency Array (LOFAR) [1] and the Square Kilometre Array (SKA) [2] have the disadvantage that the position of each antenna needs to be verified after installation. Connection problems such as switched cables will also translate to positional errors. By using signals transmitted from an Unmanned Aerial Vehicle (UAV) and received at each individual element, proposed methods such as those in [3] and [4] can accurately find the positions, compensating for inaccurate placements during the installation phase.

In [4], we specifically focused on cases where the UAV is in the near-field of the array. It was shown that the method delivers sufficiently accurate results with synthetic data, with the Root Mean Square (RMS) error less than 1% of the smallest transmitted wavelength at a signal-to-noise ratio (SNR) of $15\,\mathrm{dB}$.

In this paper, we investigate the performance of the method further with the effect of mutual coupling included, by simulating the problem in a full-wave solver, FEKO [5].

II. Sub-Sampled Exponential Analysis of the Linearised Near-Field Problem

In order to ensure that this paper is self-contained, we provide a brief summary of the mathematical details presented in [4].

The UAV transmits narrowband odd harmonic signals

$$S_i(t_p) = s_i(t_p)\exp(j\omega_i t_p)$$

towards the array at time t_p when located at position $\mathbf{r}_p = x_p\mathbf{x} + y_p\mathbf{y} + z_p\mathbf{z}$ where $s_i(t_p)$ is assumed to remain constant during the measurement of $S_i(t_p)$. The index $i \in \mathbb{N}$ distinguishes between frequencies $\omega_i = (2i+1)\omega_0$ where $\omega_0 = 2\pi f_0$ is the base frequency.

Let the reference antenna element have position $\mathbf{a}_0 = (0, 0, 0)$, coinciding with the origin. All M antenna elements are assumed to be located in the (x, y)-plane so that the m_{th} element is at position $\mathbf{a}_m = u_m\mathbf{x} + v_m\mathbf{y} + (0)\mathbf{z}$ with $m = 0, \ldots, M-1$. The UAV is in the radiating near-field of the antenna, so a curved phase front is incident on the array and the time delay of incidence on $\mathbf{a}_m$ relative to $\mathbf{a}_0$ at time t_p is

$$\begin{aligned}\tau_m(x_p, y_p, z_p) &= \frac{\|\mathbf{r}_p\| - \|\mathbf{r}_p - \mathbf{a}_m\|}{c} \\ &= \frac{r_p - \sqrt{r_p^2 + u_m^2 + v_m^2 - 2(u_m x_p + v_m y_p)}}{c},\end{aligned} \tag{1}$$

where $r_p = \|\mathbf{r}_p\|$, $\mathbf{r}_p - \mathbf{a}_m$ is the vector from the m_{th} antenna element to the UAV, and c is the propagation velocity of the signal, or the speed of light in free space.

To extract the positions $(u_m, v_m, 0)$ we collect samples at each antenna element while the UAV is at a fixed position $\mathbf{r}_p$ at time t_p, with $p = 1, \ldots, P$ [6]. Then from the narrowband assumption, the samples at the m_{th} element at time t_p for frequency i are:

$$\begin{aligned} f_{mip} &= S_i(t_p + \tau_{mp}) \\ &\approx s_i(t_p)\exp(j\omega_i t_p)\exp(j\omega_i \tau_{mp}) \\ &= s_i(t_p)\exp(j\omega_i t_p)\exp\left((2i+1)\,\Psi_{mp}\right). \end{aligned} \tag{2}$$

where

$$\begin{aligned} \Psi_{mp} &= j\omega_0 \tau_{mp}, \\ \tau_{mp} &= \tau_m(x_p, y_p, z_p) = \frac{1}{c}\left(r_p - \sqrt{r_p^2 + \Delta_{mp}}\right), \\ \Delta_{mp} &= u_m^2 + v_m^2 - 2(u_m x_p + v_m y_p). \end{aligned} \tag{3}$$

To get rid of the frequency and positional dependence in (2), we divide the sample sets f_{mip} by the reference antenna element's samples

$$f_{0ip} = s_i(t_p)\exp(j\omega_i t_p)\exp(0)$$

to give

$$f'_{mip} = \frac{f_{mip}}{f_{0ip}} = \exp\left((2i+1)\,\Psi_{mp}\right). \tag{4}$$

In the dense case where $|2\Psi_{mp}| < \pi$ and no aliasing occurs, the base terms Ψ_{mp} can be recovered from (4) using any Prony-like method. Otherwise, we use the de-aliasing method described in [4] to solve the resulting sub-sampled exponential analysis problem, which uses co-prime scale parameters $\sigma_j, j = 1, 2$. These parameters are generated from two distinct UAV flights performed at different heights z_{p_j} and overlapping planar flight paths. This gives us samples from $2P$ positions $\mathbf{r}_{p_j} = x_p\mathbf{x} + y_p\mathbf{y} + z_{p_j}\mathbf{z}$ normalised by f_{0ip_j} according to (4) at each element

$$\begin{aligned} f'_{mip_j} &= \exp\left((2i+1)\,\Psi_{mp_j}\right) \\ &= \exp\left((2i+1)\,j\frac{\omega_0}{c}\left(r_{p_j} - \sqrt{r_{p_j}^2 + \Delta_{mp}}\right)\right). \end{aligned} \tag{5}$$

The near-field base terms Ψ_{mp_j} are non-linear, so we first linearise the model with a first order Taylor series partial sum. During the linearisation $\mathbf{r}_{p_j}$ remains fixed and

$$g_{p_j}(u_m, v_m) = r_{p_j} - \sqrt{r_{p_j}^2 + \Delta_{mp}} \tag{6}$$

only varies with the planar position (u_m, v_m). We approximate (6) with

$$\begin{aligned} L_p(u_m, v_m) &= r_{p_j} - \sqrt{r_{p_j}^2 + \tilde{\Delta}_{mp}} + \frac{(u_m - \tilde{u}_m)(x_p - \tilde{u}_m)}{\sqrt{r_{p_j}^2 + \tilde{\Delta}_{mp}}} \\ &\quad + \frac{(v_m - \tilde{v}_m)(y_p - \tilde{v}_m)}{\sqrt{r_{p_j}^2 + \tilde{\Delta}_{mp}}} \\ &= \frac{u_m(x_p - \tilde{u}_m) + v_m(y_p - \tilde{v}_m)}{\sqrt{r_{p_j}^2 + \tilde{\Delta}_{mp}}} + \kappa_{mp_j} \end{aligned} \tag{7}$$

where $\tilde{\Delta}_{mp} = \tilde{u}_m^2 + \tilde{v}_m^2 - 2(\tilde{u}_m x_p + \tilde{v}_m y_p)$ and

$$\kappa_{mp_j} = r_{p_j} - \sqrt{r_{p_j}^2 + \tilde{\Delta}_{mp}} - \frac{\tilde{u}_m(x_p - \tilde{u}_m) + \tilde{v}_m(y_p - \tilde{v}_m)}{\sqrt{r_{p_j}^2 + \tilde{\Delta}_{mp}}}$$

denote the constant terms in (7) for a certain estimation $(\tilde{u}_m, \tilde{v}_m)$ of the m_{th} antenna element's true planar position. Through an iterative process, the estimation of $(\tilde{u}_m, \tilde{v}_m)$ gets updated so that the approximation in (7) becomes more accurate as the estimation gets closer to the true value of (u_m, v_m). The remaining function

$$L_p(u_m, v_m) - \kappa_{mp_j} = \frac{u_m(x_p - \tilde{u}_m) + v_m(y_p - \tilde{v}_m)}{\sqrt{r_{p_j}^2 + \tilde{\Delta}_{mp}}} \tag{8}$$

is used to solve the positions of the elements in the antenna array in the near-field sub-Nyquist case, since the common factor

$$C_{mp_j} = \frac{1}{\sqrt{r_{p_j}^2 + \tilde{\Delta}_{mp}}}$$

can be used to model σ_j, $j = 1, 2$ if we introduce the virtual UAV position $\mathbf{R}_p = x_p\mathbf{x} + y_p\mathbf{y} + Z_p\mathbf{z}$ with virtual height Z_p and $R_p = \|\mathbf{R}_p\|$, so that the spatial Nyquist criterion

$$\left|2\left(R_p - \sqrt{R_p^2 + \Delta_{mp}}\right)\right| < \frac{\lambda_0}{2} \tag{9}$$

is met for all m and p, and λ_0 is the wavelength of the base frequency f_0. Then, let

$$C_{mp} = \frac{1}{\sqrt{R_p^2 + \tilde{\Delta}_{mp}}}$$

such that

$$C_{mp_j} = \sigma_{jmp} C_{mp}. \tag{10}$$

We start the iterative process for each antenna with $\tilde{u}_m = \tilde{v}_m = 0$ so that $\tilde{\Delta}_{mp} = 0$ and $\kappa_{mp_j} = 0$. For every iteration step a new estimation of $(\tilde{u}_m, \tilde{v}_m)$ and thus $\tilde{\Delta}_{mp}$ is found, while r_{p_j} remains constant throughout. The values of σ_{jmp} and R_p get updated at every iteration step to give (10), with the only restrictions being that the spatial Nyquist criterion in (9) must be met and $\sigma_{jmp}, j = 1, 2$ must be co-prime in order to recover from aliasing. Assuming $r_{p_1} > r_{p_2}$ then $C_{mp_2} > C_{mp_1}$ for all m and p. From the ratios

$$\frac{\sigma_{2mp}}{\sigma_{1mp}} = \frac{C_{mp_2}}{C_{mp_1}} \tag{11}$$

rounded to two significant digits we get co-prime values for σ_{1mp} and σ_{2mp}. Finally, we denote

$$\begin{aligned}\sigma_{jmp}\Phi_{mp} &= j\frac{2\omega_0}{c}\left(r_{p_j} - \sqrt{r_{p_j}^2 + \Delta_{mp}} - \kappa_{mp_j}\right) \\ &\approx j\frac{2\omega_0}{c}\left(\frac{u_m(x_p - \tilde{u}_m) + v_m(y_p - \tilde{v}_m)}{\sqrt{r_{p_j}^2 + \tilde{\Delta}_{mp}}}\right) \\ &= j\frac{2\sigma_{jmp}\omega_0}{c}\left(\frac{u_m(x_p - \tilde{u}_m) + v_m(y_p - \tilde{v}_m)}{\sqrt{R_p^2 + \tilde{\Delta}_{mp}}}\right) \qquad (12)\end{aligned}$$

in order to find the unique de-aliased argument Φ_{mp} from the intersection of the two sets ($j = 1, 2$):

$$\left\{\Phi_{mp} + \frac{j2\pi}{\sigma_{jmp}}l \quad : \quad l = 0, \ldots, \sigma_{jmp} - 1\right\}. \qquad (13)$$

A new estimation for the antenna position $(\tilde{u}_m, \tilde{v}_m)$ is found using

$$\Phi_{mp} = j\frac{2\omega_0}{c}\left(\frac{r_{p_j} - \kappa_{mp_j}}{\sigma_{jmp}} - \sqrt{R_p^2 + \Delta_{mp}}\right) \qquad (14)$$

as described in [4]. The process is repeated until

$$\epsilon = \sqrt{(u_m - \tilde{u}_m)^2 + (v_m - \tilde{v}_m)^2} < 0.01.$$

A summary of the algorithm is described in Algorithm 1.

Algorithm 1 Antenna Position Estimation in the Near-Field

Initialize f_0, i, P
Collect samples f'_{mip_j} at $2P$ UAV positions as in (5)
for $m = 1$ to $M - 1$ **do**
  Compute the aliased $\exp\left(2\Psi_{mp_j}\right)$ with Root-MUSIC [7]
  Initialize $u_m \leftarrow 0$, $v_m \leftarrow 0$
  repeat
    $\tilde{u}_m \leftarrow u_m$, $\tilde{v}_m \leftarrow v_m$
    Calculate $\tilde{\Delta}_{mp}, C_{mp_j}$ and κ_{mp_j}
    Find co-prime values for σ_{1mp} and σ_{2mp} from (11)
    Find the de-aliased Φ_{mp} from the intersections in (13)
    Solve (u_m, v_m) from (14) as the intersections of circle pairs as described in [4]
  until $\epsilon < 0.01$
end for

III. Experimental Setup

Our experiment consists of a full-wave method of moment (MoM) simulation using FEKO [5]. A simple model is created to represent the 96 antennas of a LOFAR low-band antenna (LBA) sub-station. The elements are inverted-V dipoles, with the height of the vertical pole measuring $1.7\,\mathrm{m}$, and each arm having a length of $1.38\,\mathrm{m}$. Fig. 1 shows a single element as displayed in FEKO.

A voltage source of $1\,\mathrm{V}$ is added to the port of a $2\,\mathrm{m}$-long dipole, representing the UAV. Both the transmit and receive antennas have $50\,\Omega$ loads.

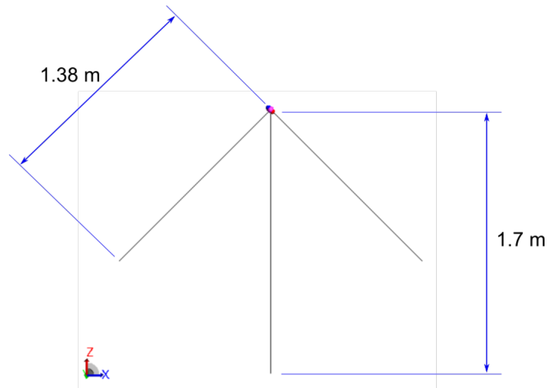

Fig. 1. Example of the inverted-V dipole antenna used as array elements in FEKO. The port is located at the end of one of the dipole arms.

A realistic flight path with $P = 16$ positions was chosen, taking on the shape of a $100\,\mathrm{m} \times 100\,\mathrm{m}$ square, slightly altered by the effect of the wind. The positions of the antenna elements, as well as the UAV flight path, are shown in Fig. 2.

The frequencies used in the simulation are $31.79\,\mathrm{MHz}$, $44.51\,\mathrm{MHz}$, $57.23\,\mathrm{MHz}$ and $69.94\,\mathrm{MHz}$. These are equivalent to the 5$^{\text{th}}$, 7$^{\text{th}}$, 9$^{\text{th}}$ and 11$^{\text{th}}$ harmonics of the base frequency $f_0 = 6.36\,\mathrm{MHz}$, meaning $i = [2, 3, 4, 5]$.

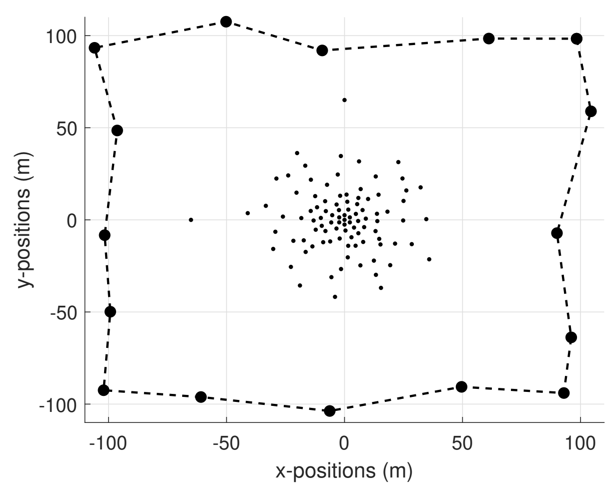

Fig. 2. Antenna positions and UAV flight path.

IV. Results

We calculate the error in position of each antenna individually in both directions, as a fraction of the smallest transmitted wavelength $\lambda_{11} = 4.3\,\mathrm{m}$. The results are shown in the middle panels of Fig. 3 and Fig. 4. The mean errors of all antenna positions in the x- and y-direction are $0.023\,\lambda_{11}$ and $0.031\,\lambda_{11}$, respectively.

In [4], at an SNR of $15\,\mathrm{dB}$, the RMS errors in both directions are smaller than $0.01\,\lambda_{11}$. It is to be expected that the results of the FEKO-simulated experiment will be less accurate than those of [4], as the physical properties are now included, leading to mutual coupling. However, the errors in Fig. 3 and Fig. 4 are sufficiently low for accurate position estimation.

To investigate further, we scale the entire array with a factor of 0.5. This means the position of each element changes from (u_m, v_m) to $\left(\frac{u_m}{2}, \frac{v_m}{2}\right)$. The element dimensions remain unchanged, as well as the UAV dimensions, flight path and frequencies. As the spacing between the elements becomes smaller, we expect the mutual coupling effects to be stronger and the results to worsen. This expectation is confirmed, as seen in the top panels of Fig. 3 and Fig. 4, where the mean errors in the x- and y-direction are $0.11\,\lambda_{11}$ and $0.098\,\lambda_{11}$, respectively. In a similar fashion, we also scale the array with a factor 1.5, to enlarge the spacing between the elements. These results are shown in the bottom panels of Fig. 3 and Fig. 4. As expected, the results have improved from the top panels, as the mutual coupling is weakened. The mean Euclidean errors of the three experiments are summarised in Table I. Here we can clearly see the trend that a larger spacing between elements leads to smaller errors.

As part of future work, we will investigate the case of switched cables in the array, and also incorporate a calibration technique to mitigate the mutual coupling effects.

TABLE I
POSITIONAL ERRORS RELATING TO ELEMENT SPACING

Scale	Mean Euclidean error (λ_{11})
0.5	0.17
1	0.042
1.5	0.038

V. CONCLUSION

In this paper, we extend the work done in [4], which described the results of the sub-sampled antenna position estimation in the near-field using synthetic data. To advance to a scenario that is truer to the practical system, we specifically focus on a simulated experiment including mutual coupling. We do this by creating a FEKO model based on the LOFAR LBA, with a UAV transmitting harmonically related signals from known positions in the sky.

The results prove to be accurate, with the mean errors in both x- and y-directions lower than 4% of the smallest transmitted wavelength. We also see how the spacing between the array elements relates to the positional error, with larger separations translating into smaller errors due to decreased mutual coupling.

Future work includes investigating the case of switched cables, incorporating a calibration method, investigating the impact of other practical effects, and testing our method with practical data of LOFAR.

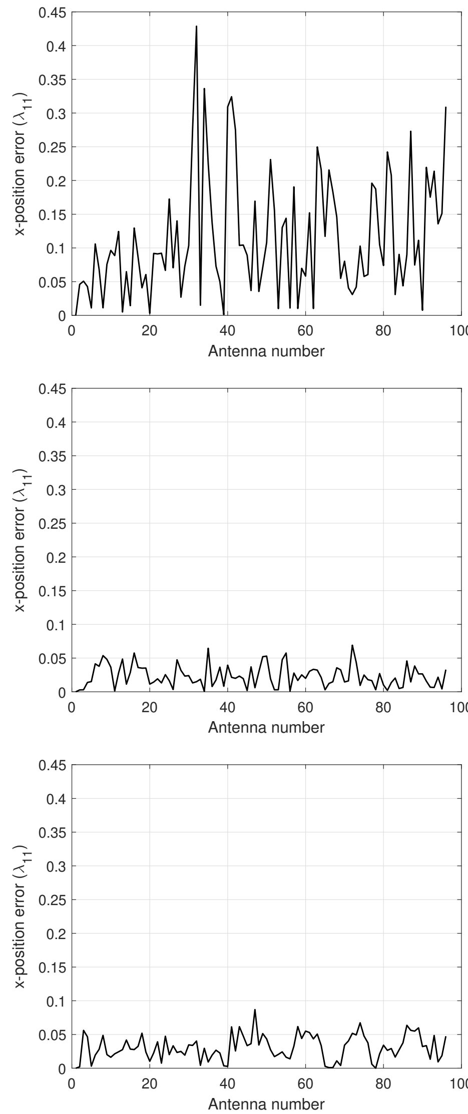

Fig. 3. Positional errors in the x-direction in terms of the smallest transmitted wavelength $\lambda_{11} = 4.3\,\mathrm{m}$. The nominal positions are scaled coordinates of the LOFAR LBA elements, with a scale factor of 0.5, 1 and 1.5 for the top, middle and bottom panels, respectively.

ACKNOWLEDGMENT

This research has received funding from the European Union's Horizon 2020 research and innovation programme under the Marie Skłodowska-Curie grant agreement No 101008231 (EXPOWER). It is also based on research supported in part by the National Research Foundation of South Africa (Grant Number 75322), as well as the Netherlands Organisation for Scientific Research.

REFERENCES

[1] M.P. van Haarlem et al., "LOFAR: The Low Frequency Array", Astronomy & Astrophysics, 556, A2, August 2013, pp. 1–53, doi: 10.1051/0004-6361/201220873

[2] P. E. Dewdney, P. J. Hall, R. T. Schilizzi, and T. J. L. W. Lazio, "The Square Kilometre Array," Proceedings of the IEEE, 97, 8, August 2009, pp. 1482–1496, doi: 10.1109/JPROC.2009.2021005.

[3] S. J. Wijnholds, G. Pupillo, P. Bolli, and G. Virone, "UAV-Aided Calibration for Commissioning of Phased Array Radio Telescopes," in URSI Asia-Pacific Radio Science Conference (URSI AP-RASC), 2016, pp. 228–231, doi: 10.1109/URSIAP-RASC.2016.7601375.

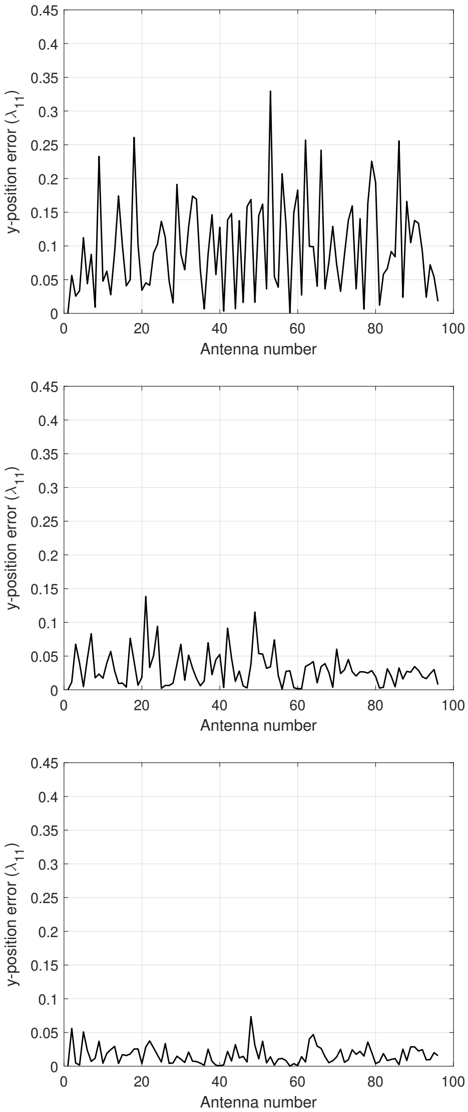

Fig. 4. Positional errors in the y-direction in terms of the smallest transmitted wavelength $\lambda_{11} = 4.3\,\mathrm{m}$. The nominal positions are scaled coordinates of the LOFAR LBA elements, with a scale factor of 0.5, 1 and 1.5 for the top, middle and bottom panels, respectively.

[4] R. Louw, F. Knaepkens, A. Cuyt, W-s. Lee, S. J. Wijnholds, D. I. L. de Villiers R. Weideman, "Antenna Position Estimation through Sub-Sampled Exponential Analysis of Signals in the Near-Field," URSI Radio Science Letters, 2022, in press.

[5] Altair Development S.A. (Pty) Ltd, Stellenbosch, South Africa. FEKO 2021.2. [Online]. Available: https://altairhyperworks.com/feko/

[6] A. Cuyt, Y. Hou, F. Knaepkens and W-s. Lee, "Sparse Multidimensional Exponential Analysis with an Application to Radar Imaging," *SIAM Journal on Scientific Computing*, **42**, 3, 2020, pp. B675-B695, doi:10.1137/19M1278004.

[7] A. Barabell, "Improving the resolution performance of eigenstructure-based direction-finding algorithms," ICASSP '83. IEEE International Conference on Acoustics, Speech, and Signal Processing, 1983, pp. 336-339, doi: 10.1109/ICASSP.1983.1172124.